

ARTICLE OPEN



Study on the oxidation resistance mechanism of self-healable NiAl coating deposited by atmospheric plasma spraying

Li Zhang¹, Di Wang¹, Xian-Jin Liao¹, Rui Chen¹, Xiao-Tao Luo¹ and Chang-Jiu Li¹✉

A dense NiAl coating with low oxide content was deposited on the GH4202 superalloy substrate by atmospheric plasma spraying (APS) using carbon-containing Ni/Al composite powders. Compared with traditional APS NiAl coatings with high oxide content, this coating exhibits better long-term oxidation resistance at 900 °C in air. For the NiAl coating with low oxide content, it was found that the improved inter-splat bonding, due to limited oxide inclusions, promotes the formation of a continuous protective Al₂O₃ layer on the coating surface during oxidation. During long-term oxidation, the dispersion of oxide scales within the coating and element diffusion across splats result in the in-situ healing of unbonded inter-splat interfaces.

npj Materials Degradation (2023)7:62; <https://doi.org/10.1038/s41529-023-00383-0>

INTRODUCTION

Ni-based superalloys are commonly used as structural components in gas turbines and aeroengines due to their superior mechanical properties at elevated temperatures^{1,2}. However, these alloys often suffer from severe oxidation problems under high-temperature service conditions, which can adversely affect their high-temperature mechanical properties³. Improving the high-temperature oxidation resistance of Ni-based superalloys is of great importance. A common method to achieve this is by preparing protective coatings on the superalloy^{4,5}. This can effectively isolate superalloy substrate from the aggressive environment, greatly reducing its oxidation rate and achieving the long life of the component in harsh conditions^{6,7}. NiAl intermetallic compounds are frequently used as protective coatings due to their excellent properties, such as high melting point, low density, excellent high-temperature oxidation and corrosion resistance^{8–10}. The protective effect mainly depends on the formation of a dense and continuous Al₂O₃ film on the coating surface during high-temperature oxidation¹¹. Due to the unique advantages of the NiAl coatings, they are used as a bond coat in multilayer thermal barrier coating systems in temperature regions > 1200 °C¹², such as the combustion chambers of gas turbines and first stages of turbine blading¹³. Additionally, NiAl coatings are used as a monolayer coating to provide oxidation protection for the substrate material^{14,15}. For instance, in compressor blades that experience temperatures lower than 900 °C, the monolayer coating can be used without the need for a ceramic topcoat¹⁶.

In general, the NiAl coatings can be deposited using various processes, including thermal diffusion of Al into Ni-based alloys¹⁷, electron beam physical vapor deposition (EB-PVD)¹⁸ and thermal spraying¹⁹. Among these processes, thermal spraying is a versatile, simple and low-cost approach. Among the various thermal spraying technologies, atmospheric plasma spraying (APS) has been widely used to deposit various protective coatings due to its low cost and high efficiency²⁰. However, metal powders are easily oxidized in the high-temperature plasma jet during spraying, leading to severe oxide inclusions at the inter-splat boundaries and resulting in the formation of through-thickness pores within the coating^{21,22}. Such through-thickness pores can

act as the fast pathway of the oxidative media, making the porous NiAl coating less protective against high-temperature oxidation. It has been shown that high oxide content and pores in APS NiAl coatings easily promote the formation of mixed-oxide layers on their surfaces during isothermal oxidation²³. Therefore, the APS NiAl coatings usually show poor oxidation resistance at high temperatures due to the high growth rate of mixed oxides. This significantly limits the application of the APS process for the preparation of NiAl coatings. So far, several methods have been investigated to improve the oxidation of metal elements during APS and achieve fully dense coatings, such as vacuum plasma spraying²⁴, shrouded plasma spraying²⁵ and adding elements with a strong affinity for oxygen into metal powders²⁶. Our previous work has reported that the addition of the carbon deoxidizer can effectively suppress the oxidation of APS NiAl coatings²⁷. According to the proposed theory that carbon can preferentially react with oxygen at high temperatures (T > 2000 °C) relative to Ni and Al elements, oxide-free NiAl molten droplets and thereby dense NiAl intermetallic compound coating with low oxygen content can be achieved. It is even more interesting to investigate how the oxide inclusions influence the oxidation behavior of the NiAl coating in the high-temperature ambient atmosphere.

In the present work, NiAl coating with a dense microstructure and low oxygen content was deposited onto GH4202 by APS technique using diamond-added NiAl composite powder. We examined the high-temperature oxidation behavior of this coating in comparison to the traditional NiAl coating with a high oxide content. The samples were isothermally oxidized at 900 °C at different periods to study the microstructural evolution, oxidation kinetics and long-time oxidation resistance of the coatings. Additionally, the oxidation protection mechanism of the coatings was discussed.

RESULT AND DISCUSSION

Microstructural features of the as-sprayed NiAl coatings

Figure 1 shows the microstructures of the NA0 coating and NA1 coatings deposited by APS. The NA0 coating prepared using Ni/Al

¹State Key Laboratory for Mechanical Behavior of Materials, School of Materials Science and Engineering, Xi'an Jiaotong University, Xi'an, Shaanxi province 710049, China.

✉email: licj@mail.xjtu.edu.cn

powder has a high oxide content and high porosity of 4.9% (Fig. 1a). In contrast, the NA1 coating prepared using Ni/Al powder with 2 wt% diamond exhibits fewer oxide inclusions, denser microstructure, and reduced porosity of 2.3% (Fig. 1b). Figure 1c and d show the microstructure of the NA0 and NA1 coatings at a higher magnification. The NA0 coating shows obvious unbonded splat interface gaps and oxides between the interlayers (Fig. 1c). When the diamond as a carbon source is added to the powder, only a small amount of oxide inclusions were observed within the coating, and weakly bonded interfaces between the interlayers were limited (Fig. 1d). These oxides possibly result from the in-flight oxidation of small molten droplets and the unbonded interfaces were evolved due to limited wetting of high melting point intermetallic compounds during splatting with rapid cooling. Due to the in-situ in-flight deoxidizing effect of the ultra-high temperature carbon-containing NiAl droplets during plasma spraying, most of the in-flight droplets can maintain oxide-free state²⁷. The oxygen content of the coatings was measured using an oxygen, nitrogen, and hydrogen analyzer, and it was found that the addition of 2 wt% diamond as carbon source significantly reduced the oxygen content of the coating from 3.23 wt% to 0.61 wt %, resulting in a denser microstructure.

Isothermal oxidation behavior of the NA0 and NA1 coatings

XRD patterns of the NA1 and NA0 coatings after isothermal oxidation for different durations are shown in Fig. 2. As seen in Fig. 2a, a single-phase Al_2O_3 layer forms on the NA1 coating surface during isothermal oxidation. Mixed oxides including NiO and NiAl_2O_4 were not detected throughout the isothermal oxidation. The intensity of the peaks for $\alpha\text{-Al}_2\text{O}_3$ showed only a slight increase with increasing oxidation duration, possibly due to the limited increase in oxide scale thickness. Furthermore, compared to the XRD of as-sprayed NA1 coating, a large amount of NiAl phase in the near-surface layer of the coating transforms into the lower Al-containing phase Ni_3Al after 10 h, and the Ni_3Al content increases with increasing oxidation time. This is due to the outward diffusion of Al from the near-surface layer of the NA1 coating during isothermal oxidation, which leads to the formation of Al_2O_3 on the coating surface and the continuous consumption of Al.

Figure 2b shows the XRD patterns of the as-sprayed NA0 coating after isothermal oxidation. It can be observed that in addition to Al_2O_3 , mixed oxides including NiAl_2O_4 and NiO were formed on the NA0 coating surface during isothermal oxidation at 900 °C. This could be due to the severe in-flight oxidation of Al elements during APS, which consumes a large amount of Al and reduces the Al content in the coating. In addition, the high

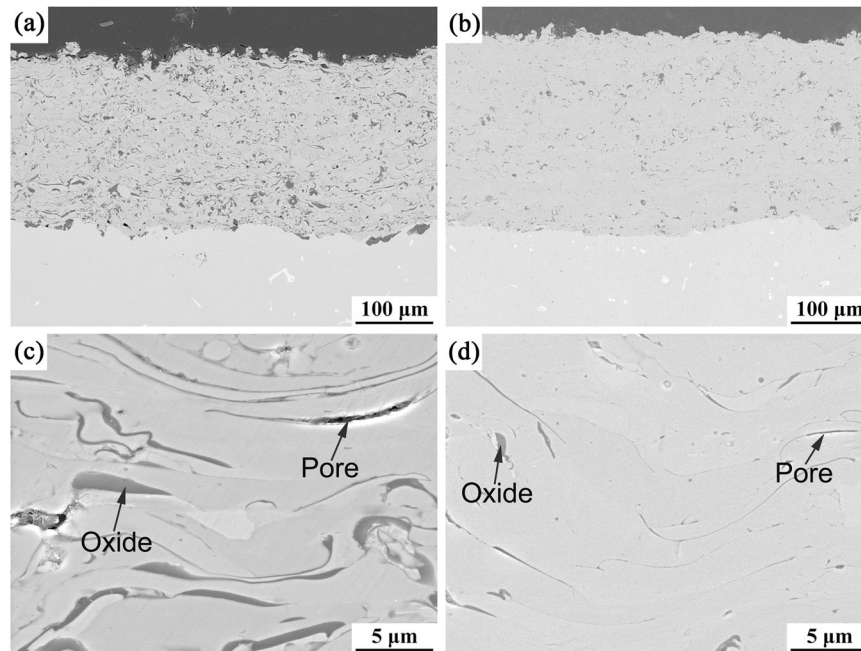


Fig. 1 Cross-sectional microstructure of the coatings. **a, c** NA0 coating; **b, d** NA1 coating.

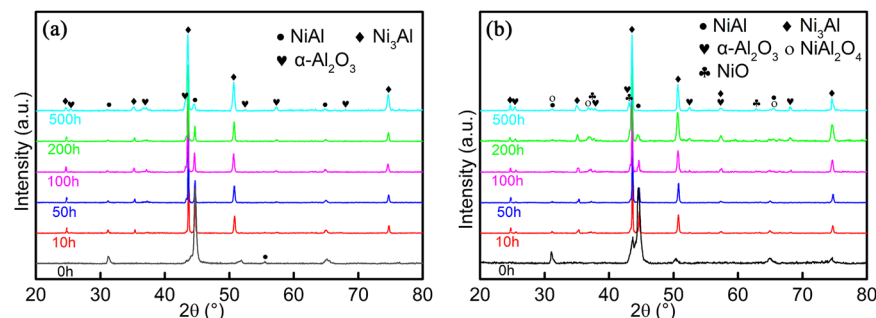


Fig. 2 XRD patterns of the coatings after isothermal oxidation for different durations showing the structure of oxide scales on the coating surface. **a** NA1 coating; **b** NA0 coating.

porosity of the NA0 coating and poor inter-splat bonding caused by severe oxidation provide channels for the continuous permeation of oxygen gas into the coating during the isothermal oxidation, resulting in internal oxidation of the NA0 coating and further limiting the diffusion of Al towards the coating surface. When the supply of Al is insufficient, Ni in the coating diffuses outward and reacts with oxygen to form NiAl_2O_4 and NiO on the NA0 coating surface.

Figure 3 shows the cross-sectional microstructure of the oxide layer formed on the dense NA1 coating with a low oxygen content subjected to isothermal oxidation for different durations. For comparison, the cross-sectional microstructures of the GH4202 substrate and the NA0 coating after the same isothermal oxidation are shown in Fig. 4 and Fig. 5, respectively. As can be expected from the literature²⁸, severe oxidation occurred in the superalloy, resulting in the formation of mixed oxide layers on the

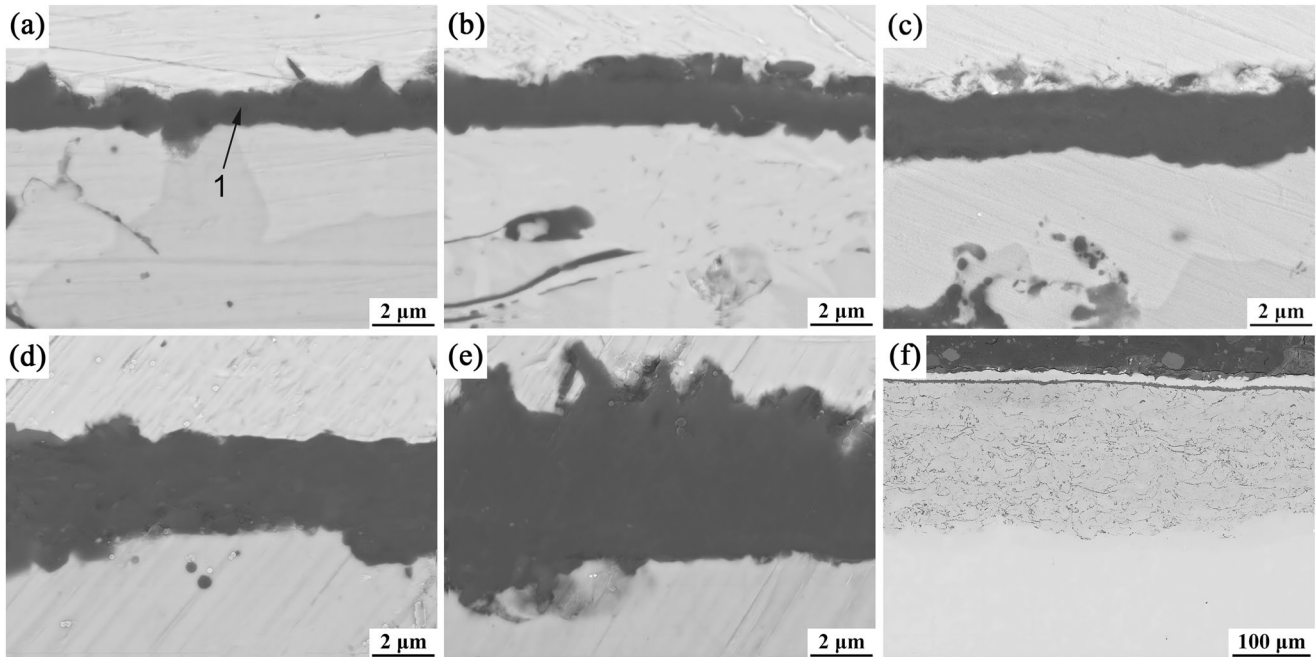


Fig. 3 Cross-sectional microstructures of oxide scales formed on the surface of APS NA1 coating with limited oxide inclusion after oxidation at 900 °C for different times. **a** After 10 h; **b** After 50 h; **c** After 100 h; **d** After 200 h; **e** After 500 h; **f** Low magnification to show the full image of the coating after oxidation for 500 h.

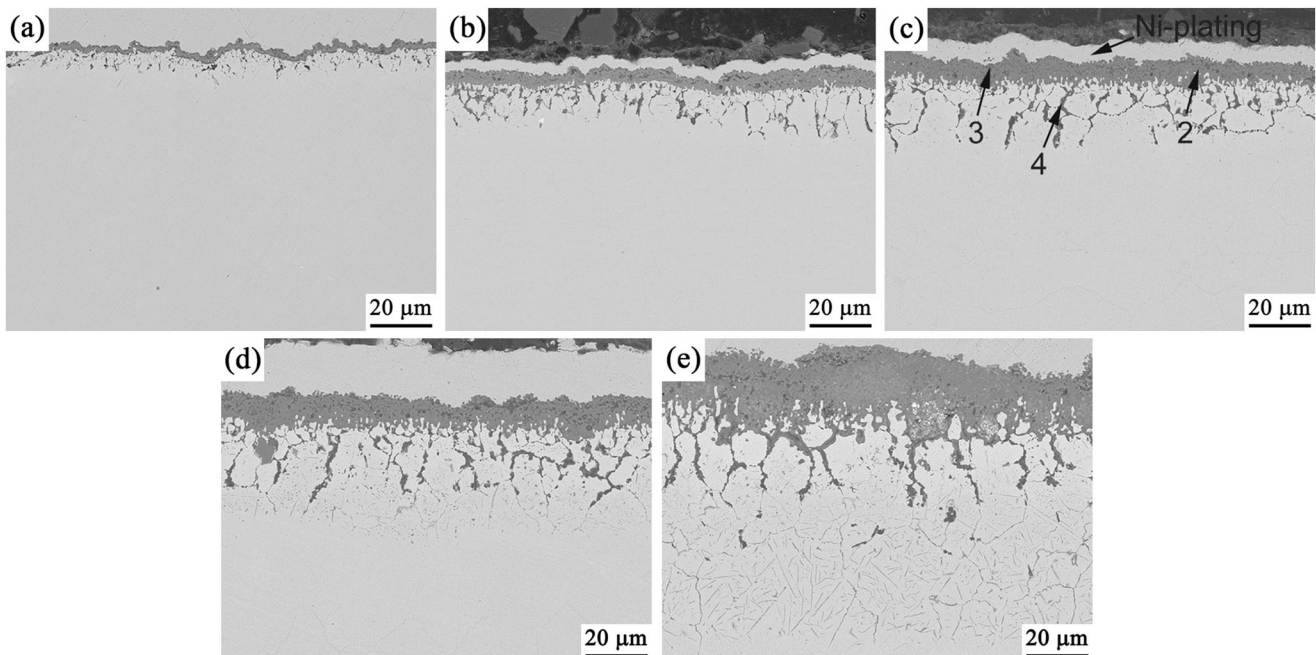


Fig. 4 Cross-sectional microstructures of oxide scales formed on the surface of the Ni-based GH4202 superalloy substrate after oxidation at 900 °C for different times. **a** After 10 h; **b** After 50 h; **c** After 100 h; **d** After 200 h; **e** After 500 h.

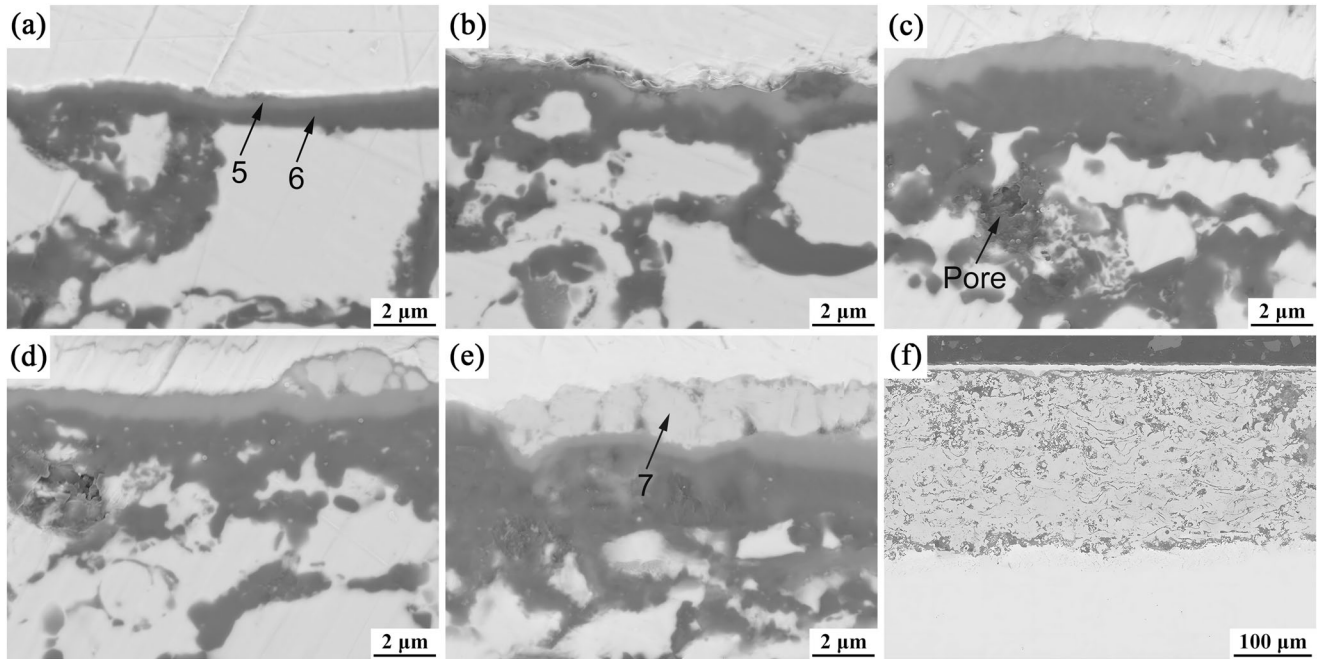


Fig. 5 Cross-sectional microstructures of oxide scales formed on the surface of APS NAO coating having high content oxides after oxidation at 900 °C for different times. **a** After 10 h; **b** After 50 h; **c** After 100 h; **d** After 200 h; **e** After 500 h; **f** Low magnification to show the full image of the coating after oxidation for 500 h.

Regions	Ni/at.%	Cr/at.%	Ti/at.%	Al/at.%	O/at.%
1	2.77	0	0	38.93	58.30
2	2.35	37.66	0	0	59.99
3	2.52	8.54	23.42	0	65.52
4	29.29	6.06	1.20	25.69	37.76
5	14.16	0	0	29.84	56.00
6	2.12	0	0	37.56	60.32
7	47.01	0	0	1.02	51.97

GH4202 surface after oxidation at 900 °C, as shown in Fig. 4. The EDS results in Table 1 suggest that the oxide scale on the GH4202 surface consists of the Cr-rich and Ti-rich mixed oxides, as well as the internal Al-rich oxide. Although Cr₂O₃ film can prevent further oxidation of alloy, its protective function for superalloy oxidation may degenerate, because the Cr₂O₃ film becomes loose due to the presence of Ti oxide. It can be seen that the oxide layer generated on the surface of GH4202 appears to be continuous during isothermal oxidation. However, the GH4202 substrate is not well protected. Even in the early stages of oxidation, oxidation has already developed into the substrate below the oxide layer and formed an internal oxidation zone. As the oxidation duration increases, the thickness of the oxide scale gradually increases and the internal oxidation along the grain boundaries of the GH4202 substrate becomes increasingly severe. Such oxidation along grain boundaries can significantly degrade the strength of the superalloy.

For the dense NA1 coating, as shown in Fig. 3, a uniform oxide scale formed on the coating surface. The oxide scale consisted of a monolayer oxide throughout the isothermal oxidation, and its thickness gradually increased with increasing oxidation time. The EDS results in Table 1 show that this monolayer oxide contains

only Al and O elements, which indicates that this monolayer oxide is Al₂O₃. This is consistent with the XRD results in Fig. 2a. The SEM image of the whole coating after 500 h of oxidation, shown in Fig. 3f, demonstrates that further diffusion of oxygen into the coating is prevented due to the protective Al₂O₃ scale formed on the surface of NA1 coating. Therefore, even after 500 h of oxidation, no significant internal oxidation occurs within the NA1 coating.

In contrast, for the NAO coating with a high content of oxides, as shown in Fig. 5 after oxidation, the oxide scales formed on the coating surface are divided into two layers with significantly different contrasts. The EDS results in Table 1 show that Ni, Al and O elements are present in the outermost layer, while the inner oxide layer mainly consists of O and Al. This suggests that the outer oxide layer is NiAl₂O₄, and the inner layer is Al₂O₃, being consistent with the XRD results in Fig. 2b. As the oxidation time increases to 200 h, non-uniform protrusion appears on the outermost layer of the oxide scales. Combined XRD and EDS results (point 7) indicate that the protrusion is NiO. This result indicates the insufficient amount of Al content within the coating to maintain the formation of the protective Al₂O₃ scale on the surface. The non-uniform NiO on the NAO coating surface becomes more significant with a further increase in the oxidation time to 500 h. Moreover, visible pores are present in the oxide scale, indicating that the mixed oxides formed on the surface of the NAO coating did not provide reliable protection and permitted oxygen permeation to occur⁹. As a result, severe oxidation of the metal coating occurs throughout the splats beneath the porous oxide scale and within the coating. The whole cross-sectional image of the coating after 500 h of oxidation, as shown in Fig. 5f, clearly demonstrates that severe internal oxidation has occurred in the coating and even occurred at the coating/superalloy substrate interface.

Generally, materials with excellent high-temperature oxidation resistance are attributed to the formation of a dense Al₂O₃ layer which does not permit the permeation of gaseous oxygen with a low atomic oxygen diffusivity. Figure 6 shows the relationship between the isothermal oxidation time and the oxide layer thickness on the surface of dense NA1 coating, compared to the

GH4202 superalloy substrate. The linear fitting to each set of data points against the square root of time indicates that the growth of the oxide layer substantially follows the parabolic growth law. The NA1 coating exhibits a parabolic growth rate constant of $0.23 \mu\text{m}/\text{h}^{1/2}$, which is comparable to that of the NiAl-based alloy reported in other studies²⁹. In contrast, the GH4202 substrate shows a high oxidation rate constant of $0.64 \mu\text{m}/\text{h}^{1/2}$, which is about three times that of the NA1 coating. This is typical of the cyclic oxidation kinetics of chromium-forming superalloys like

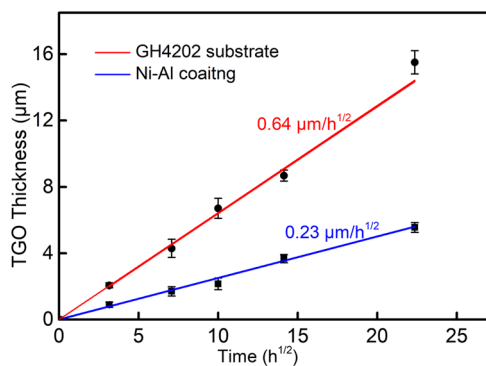


Fig. 6 Curves of oxide layer thickness varying with isothermal oxidation time.

GH202 and Rene-80^{28,30}, and can be attributed to the higher diffusivity of oxygen through the Cr_2O_3 scale than through the Al_2O_3 scale³⁰. Therefore, the uncoated GH4202 substrate exhibited poor oxidation resistance at 900°C . It is difficult to measure the oxide layer thickness of the NA0 coating at different oxidation times due to the severe oxidation of the metal elements below the oxide layer during the isothermal oxidation.

Transient internal oxidation and inter-splat interface oxide healing behavior

Traditional plasma-sprayed metallic coatings inevitably experience internal oxidation when exposed to high temperatures, due to severe oxidation and high porosity that create through-thickness passages for the gaseous or liquid substances to penetrate to the substrate-coating interface, which will influence the durability of the coatings^{31–33}. Figure 7 shows the cross-sectional microstructure of the NA1 coating after isothermal oxidation at 900°C for 1 h, 10 h, 50 h, 100 h, 200 h and 500 h. Compared to only very limited lens-shaped oxides in the as-sprayed coating (Fig. 1d), many dark gray oxide films are observed at the interlayer interfaces in the coating after short-term oxidation for 1 h (Fig. 7a), and the EDS line scanning result indicates the formation of an Al oxide (Fig. 7g). Such oxide films are formed when the coating is exposed to the ambient high-temperature oxidation atmosphere. As mentioned above, although the in-flight oxidation of the spray particles is successfully suppressed by adding diamond as a carbon source,

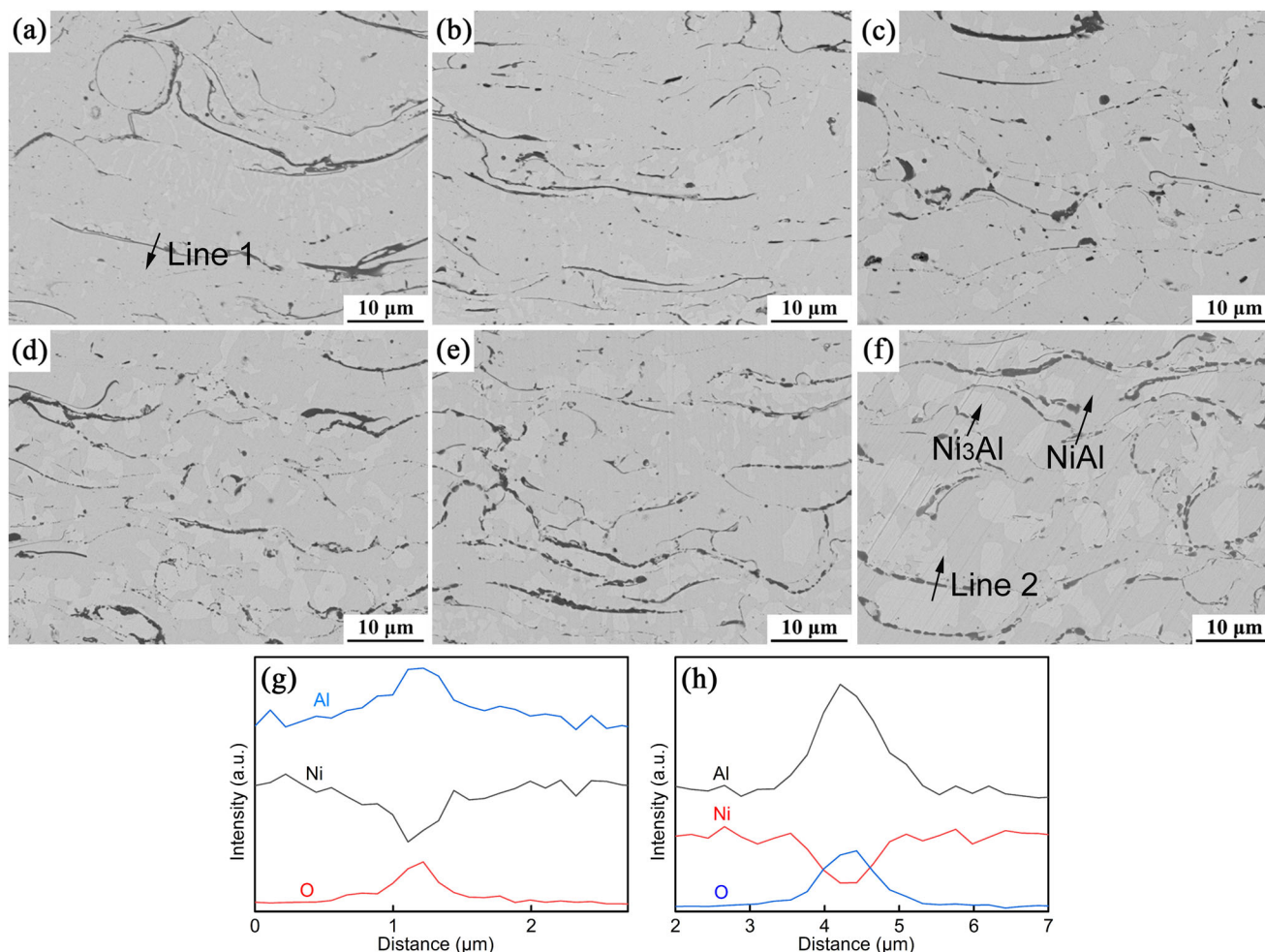


Fig. 7 Cross-sectional microstructures of the interlayer oxides in NA1 coating after oxidation at 900°C for different durations and EDS results. **a** After 1 h; **b** After 10 h; **c** After 50 h; **d** After 100 h; **e** After 200 h; **f** After 500 h; Line scanning of interlayer oxides in the coatings in Fig. 7a (**g**) (Line 1) and Fig. 7f (**h**) (Line 2).

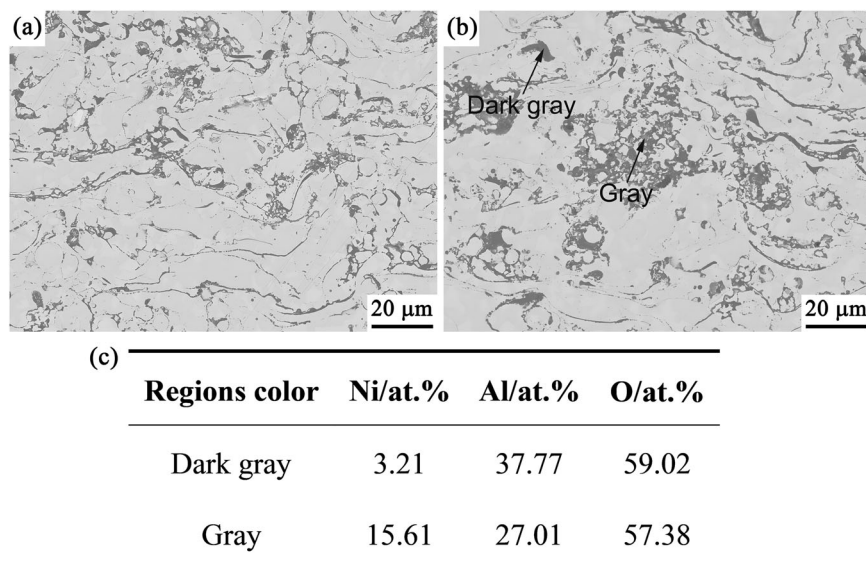


Fig. 8 Cross-sectional microstructures of NAO coating after oxidation at 900 °C for different durations. **a** After 10 h; **b** After 500 h; **c** EDS results in Fig. 8 (b).

the temperature of the in-flight particles is limited by Al evaporation. Therefore, fully metallurgical bonding across all inter-splat interfaces is not formed when the molten NiAl droplets impact on the deposited NiAl coating. Because the droplets generated during plasma spraying can create impact-induced melting and subsequently metallurgical bonding only if they are overheated to a high enough temperature. Weakly bonded interfaces are still present in the NA1 coating (Fig. 1d). During early isothermal oxidation, these weakly bonded interfaces act as channels for the permeation of oxygen into the coating. Thus, oxygen permeates into the interior of the coating. These oxygens react with the surrounding active metal elements on the splat surface. Compared to Ni, the reaction of Al with oxygen has low free energy, leading to the selective oxidation of Al occurring first at the weakly bonded interface during the early stage of isothermal oxidation. As the oxidation time increases from 1 h to 10 h (Fig. 7b) and 50 h (Fig. 7c), there is no aggravation of internal oxidation of the coating, indicating that the diffusion of oxygen into the NA1 coating is prevented during this period. This is mainly attributed to the formation of a continuous protective Al_2O_3 layer on the NA1 coating surface (Fig. 3). Additionally, it can be observed that the NiAl phase adjacent to the oxide in the coating gradually transformed into the Ni_3Al phase due to the consumption of Al element. It is worth noting that the dispersion of some thinner oxide films at the inter-splat interfaces occurred as the isothermal oxidation time increased to 100 h (Fig. 7d). The oxides changed from a smooth film (Fig. 7a and b) to discontinuous oval-shaped oxide inclusions. However, the thicker oxide film still maintained a smooth and continuous morphology. When the isothermal oxidation time was increased to 200 h (Fig. 7e), the thicker oxide film maintained its continuity, and its morphology became uneven and exhibited a jagged shape. It is not until 500 h that the dispersion of some thicker oxide film in the coating also occurred, and it experienced a longer breaking period compared to the thinner oxide film (Fig. 7f). When the continuous oxide scales at the inter-layer interfaces transformed into isolated oxide particles, the interface between the lamellar splats was healed and the metal elements could diffuse freely within the coating.

Due to the high porosity and oxide inclusion content of the NAO coating, oxygen can quickly penetrate into the coating. Non-protective mixed oxides are formed on the NAO coating surface during isothermal oxidation. Therefore, as shown in Fig. 8a, severe internal oxidation of the coating occurred even after only 10 h of

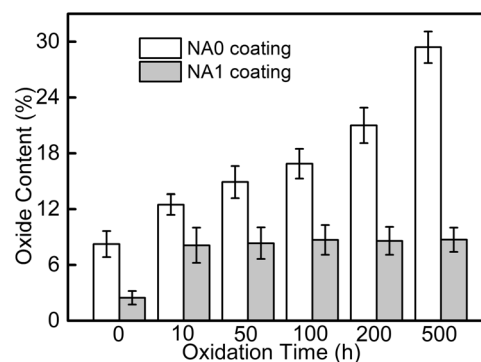


Fig. 9 Oxide content of the NAO and NA1 coatings after the isothermal oxidation for different durations.

isothermal oxidation. Dark oxide films were clearly observed along the boundaries of splats, and with increasing oxidation time up to 500 h, the internal oxidation of the coating became even more severe. EDS analysis listed in Fig. 8c showed the presence of Ni, Al and O elements in the oxides formed within the coating during isothermal oxidation. The content of these elements in different areas was not the same. Based on the EDS results, the dark gray regions were identified as Al_2O_3 , while the gray region corresponded to NiAl_2O_4 . Evidently, the formation of high content NiAl_2O_4 with a porous feature does not provide an effective barrier to suppress the permeation of gaseous oxygen and prevent coating internal oxidation.

Figure 9 shows the oxide content of the NAO and NA1 coatings after the isothermal oxidation for different durations. The statistical oxide content of the as-sprayed NAO and NA1 coatings was 9.1% and 2.2%, respectively. The oxide content in the NAO coating increased gradually with an increase in the isothermal oxidation time almost linearly, and after oxidation for 500 h, the oxide content of the NAO coating increased to 29.4%. However, the oxide content in the NA1 coating only increased from 2.2% to 8.1% after oxidation for 10 h, and there is no significant change was observed in the oxide content of NA1 coating with further isothermal oxidation. This suggests that a large amount of Al is retained in the metallic phase of the coating, and sufficient Al is beneficial to the formation of Al_2O_3 on the coating surface. The

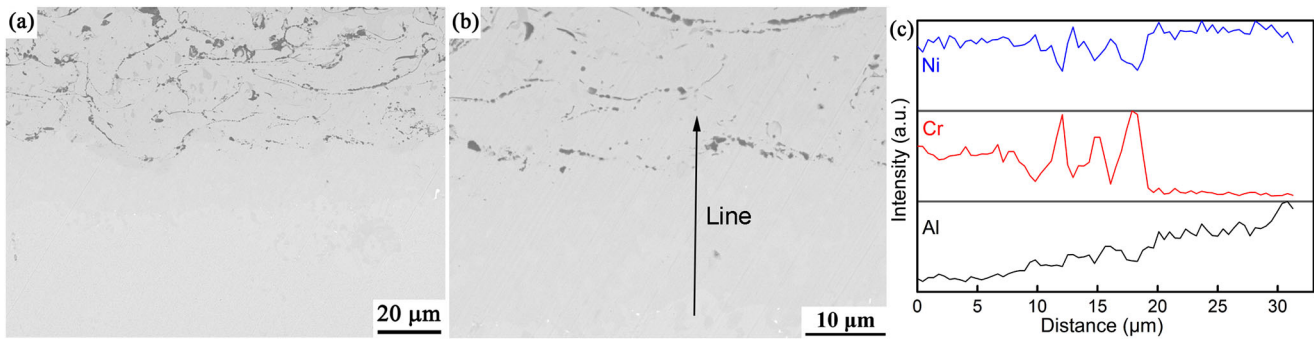


Fig. 10 Cross-sectional microstructure and EDS result. **a, b** Cross-sectional microstructure of NA1 coating/GH4202 substrate after oxidation at 900 °C for 500 h; **c** Line scanning of NA1 coating/GH4202 substrate interface.

Al_2O_3 formed on the NA1 coating surface during isothermal oxidation provides an effective barrier that prevents the diffusion of oxygen into the interior of the coating and suppresses the oxidation of the NA1 coating.

Oxidation behavior of the NiAl coatings/GH4202 substrate interface

As mentioned above, when the NA1 coating with low oxide content and dense microstructure is deposited on the Ni-based GH4202 superalloy substrate, a protective Al_2O_3 scale can be formed on the coating surface, and the initial internal oxidation within the coating is gradually suppressed during isothermal oxidation. This protection effectively prevents the oxidation of GH4202 in high-temperature environments. As shown in Fig. 10a, no oxides were observed between the NA1 coating and GH4202 substrate interface after 500 h, and the coating became metallurgically bonded to the substrate through oxide dispersion and element diffusion across the interface. Figure 10c shows the EDS line scanning results along line L1 across the NA1 coating/GH4202 substrate interface in Fig. 10b. It is clear that the Al element has diffused from the NiAl coating into the GH4202 substrate with a diffusion depth of about 20 μm . This may have a negative effect on the formation of Al_2O_3 on the coating surface if the Al content in the coating is too low with a thin coating. In this case, NiAl_2O_4 and NiO may form on the coating surface during isothermal oxidation^{34–36}. However, the present thick NA1 coating, as revealed by the XRD pattern in Fig. 2a, no significant Al depletion was presented near the surface region. As a result, a single Al_2O_3 grows on the coating surface, effectively protecting the GH4202 substrate from oxidation.

Figure 11 shows the microstructures of the NAO coating/GH4202 substrate interface after isothermal oxidation for 500 h, as well as the corresponding distributions of major elements. Due to the high porosity and the poor inter-splat interface bonding caused by severe oxidation of the NAO coating, oxygen can easily enter the interior of the coating from the external air and reach the coating/substrate interface through these defects. Therefore, in addition to the severe internal oxidation of the coating, the GH4202 substrate was also severely oxidized during the isothermal oxidation, the mixed oxides of Ni, Cr, Al and O were formed at the coating/GH4202 substrate interface, and the oxidation along the grain boundaries of the GH4202 superalloy substrate below the mixed oxides was observed, as observed in Fig. 11. This result indicates that the conventional NAO coating with high oxide content is not able to protect GH4202 from high-temperature oxidation in an ambient atmosphere. Moreover, the phase with acicular structure was observed to precipitate in a thickness range of approximately 50 μm below the coating/GH4202 substrate interface oxides. Based on the relevant studies^{37–39} and EDS results in Fig. 11, it can be considered that

the phase of the acicular structure is TiN, which is harmful to the oxidation scale stability, especially in Ti-containing⁴⁰.

Discussion on the oxidation protection mechanism

Plasma-sprayed coating always presents a typical lamellar structure since the coatings are formed by the successive impact of molten droplets. The oxides in in-flight NiAl droplets and on previously deposited NiAl splat surfaces degrade the wettability of the spreading droplet and subsequently hinder the bonding formation between inter-lamellar interfaces within the coating. Accordingly, a certain amount of porosity is present in NiAl coating. In this study, by adding diamond as a carbon deoxidizer to Ni/Al composite powder, the oxide content of the NiAl coating is reduced significantly and the compactness of the coating is also greatly increased. However, sufficient metallurgical bonding between splat interfaces, which can be effectively achieved by the spread-fusing mechanism through highly over-heated molten droplets⁴¹, cannot be expected due to the high melting point of NiAl alloy. Therefore, there are still some weakly bonding interfaces within the APS NA1 coating despite limited oxide films between inter-splat interfaces. Interestingly, in-situ healing of inter-lamellar interfaces was observed during high-temperature exposure, even under an oxidizing atmosphere. As a result, the low oxide and dense NA1 coating effectively protected the metal substrate from high-temperature oxidation. Conversely, internal oxidation occurred throughout the oxidation test duration for the NAO coating with high oxide content, resulting in severe oxidation of the GH4202 substrate. Thus, conventional NAO coatings do not provide effective protection against oxidation. However, even with the low oxide content NA1 coating, effective protection depends on the formation of a continuous and protective Al_2O_3 scale and inter-splat interface healing. Therefore, the interfacial microstructure evolution of the coating is of essential importance for its high-temperature oxidation protection.

Based on the oxidation behavior of two NiAl coatings in this study, the protection mechanism of the APS NA1 coating can be shown schematically in Fig. 12, in comparison with the APS NAO coating. The high oxide inclusion in the NAO coating (Fig. 1a and c) results in limited inter-splat bonding and high porosity. The pores along with porous oxides act as inter-connected channels for oxygen transportation through the coating to the GH4202 substrate. During isothermal oxidation, oxygen infiltrates into the coating and the coating/GH4202 substrate interface along the inter-connected pores, leading to oxidation of the coating and superalloy. Then, the internal oxides will form within the open pores and inter-splat gaps in the coating and the GH4202 superalloy substrate is oxidized simultaneously (Fig. 12a). As the oxidation time increases, the open pores within the coating are not completely closed, allowing oxygen to reach the coating/substrate interface, and causing more severe oxidation of the GH4202 substrate (Fig. 12a). The internal oxidation of the NAO

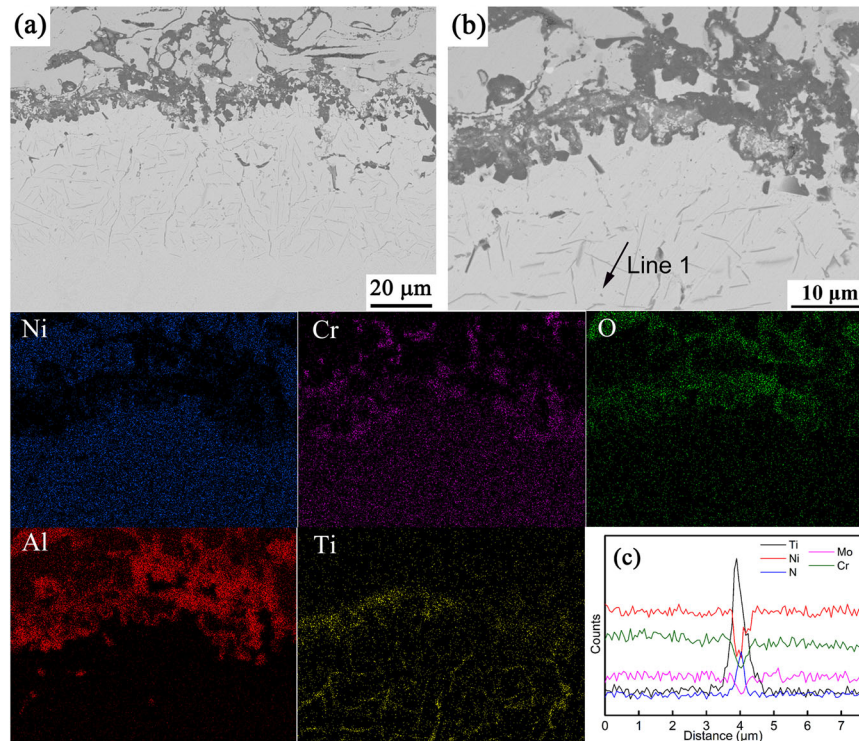


Fig. 11 Cross-sectional microstructure and EDS result. **a** Cross-sectional microstructure of NAO coating/GH4202 substrate after oxidation at 900 °C for 500 h; **b** Partially enlarged image of Fig. 11a; **c** EDS result of Line 1.

coating affects the formation of a protective Al_2O_3 scale on the coating surface. Previous results⁴² have shown that the formation of the protective Al_2O_3 layer on the coating surface depends on a continuous supply of Al elements. During APS, some Al elements are consumed by oxidation. Severe internal oxidation of the coating during thermal exposure also consumes a large amount of Al, preventing the continuous supply of Al elements from the inside to the surface of the NAO coating. In case of insufficient Al supply or not quick enough diffusion of Al atoms from the internal coating toward the coating surface, Ni in the coating diffuses outward and reacts with oxygen to form mixed oxides such as NiAl_2O_4 and NiO due to selective oxidation³⁵. As the oxidation time increases, the internal oxidation of the coating becomes more severe, resulting in the further depletion of Al elements. Additionally, a porous NiO layer grows on the coating surface (Fig. 12a).

The NA1 coating exhibits a compact microstructure with few defects due to significantly suppressed in-flight oxidation (Fig. 1b and d) and thus has excellent oxidation resistance. As shown in Fig. 12b, during early oxidation, the coating undergoes slight internal oxidation at some unbonded inter-splat interfaces, forming a small amount of the Al_2O_3 scales within the coating. This hinders further oxygen permeation into the coating (Fig. 12b), and the coating surface is oxidized continuously at the same time. Better inter-splat contact leads to the continuous supply of Al from sub-surface splats towards the surface through diffusion for the growth of the protective Al_2O_3 scale on the NA1 coating surface. In addition, due to the blockage of smaller interfaces by in-situ formed dense Al_2O_3 within the coating, internal oxidation mainly occurs at unbonded splat interfaces with large openings, leading to the presence of thick oxide scales in the coating. At the same time, the unbonded interfaces isolated without oxygen access start to heal.

As the entire top surface of the coating is covered by a conformal, dense Al_2O_3 scale, the permeation of gaseous oxygen from open air is blocked. As the oxidation time further increases,

the continuous oxide film generated by initial internal oxidation within the coating undergoes breaking (Fig. 12b). Based on Thompson's research, the solid films are usually unstable in the as-deposited state and they break to form islands when heated to sufficiently high temperatures. This process is driven by surface energy minimization and can occur via surface diffusion well below the melting temperature of a film⁴³. Meng et al. also demonstrated the transformation of lamellar oxides presented between the splats within the as-sprayed APS coatings into isolated oxide particles when the heat treatment is carried out in low oxygen partial pressure conditions⁴⁴. Meanwhile, the dispersion time of the oxide film exhibited a linear relationship with the thickness of the oxide film^{45,46}. Since a continuous and dense Al_2O_3 scale evolves on the NiAl coating surface, preventing the diffusion of oxygen into the coating, which creates low oxygen partial pressure conditions within the coating, causing the continuous oxide scale to break and subsequently disperse during later isothermal oxidation. For oxide films of different thickness values, under the same oxidation temperature and time, the dispersion completes earlier for thinner oxide film, while the thicker oxide film will also experience breakage as the oxidation time increases. The dispersion of continuous Al_2O_3 films between the interlayer leads to the rapid diffusion of metal elements across splat interfaces within the coating. As a result, the protective Al_2O_3 scale continues to grow on the coating surface due to the diffusion of large amounts of Al element, suppressing the formation of the mixed oxide such as NiAl_2O_4 and NiO . Therefore, the NA1 coating exhibits excellent long-term high-temperature oxidation resistance.

In summary, we deposited the NA1 coating on the GH4202 Ni-based superalloy substrate by APS using mechanically-milled Ni/Al/2wt.%diamond composite powder. The oxidation behavior of the coating was investigated at 900 °C in an ambient air atmosphere in comparison with the conventional APS NAO coating plasma-sprayed with Ni/Al composite powder. The following conclusions can be drawn:

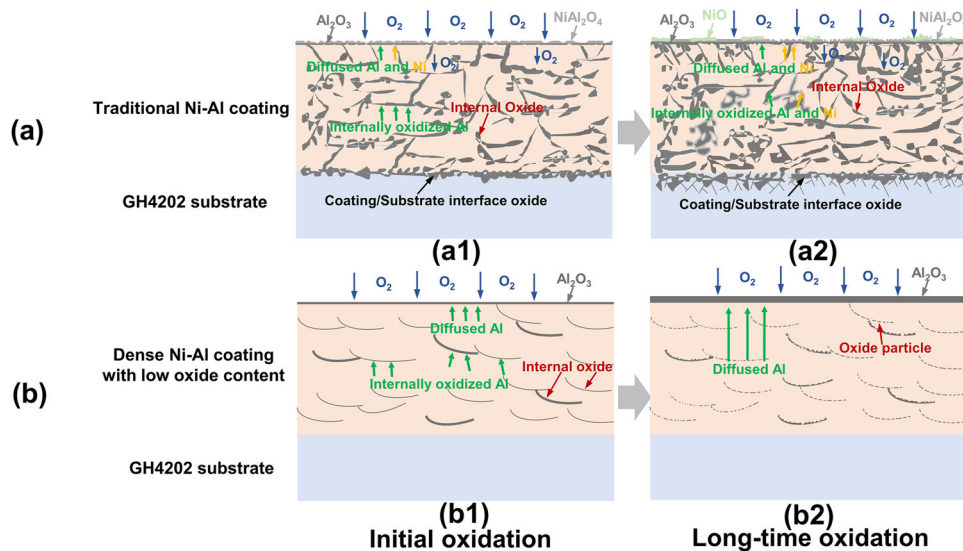


Fig. 12 Oxidation schematic diagram of the APS Ni-Al coatings. **a** Traditional Ni-Al coating; **b** Dense Ni-Al coating with low oxide content.

By adding 2 wt.% of diamond into the Ni/Al composite spray powder, a dense NA1 coating with a low oxide inclusion content of 2.2% and porosity of 2.3% was achieved by APS, through the in-flight deoxidizing effect of the carbon-containing droplets, compared to the conventional NiAl coating with the oxide inclusion of 9.1% and porosity of 4.9%.

A protective Al_2O_3 scale can be formed on the NA1 coating surface during direction oxidation at 900°C in the air atmosphere, while no protective oxide scale was formed on the conventional NiAl coating deposited by NiAl composite powders. The NA1 coating presented an oxidation rate constant of $0.23\ \mu\text{m}/\text{h}^{1/2}$, which is only about 1/3 of the $0.64\ \mu\text{m}/\text{h}^{1/2}$ obtained for the Ni-based GH4202 superalloy substrate.

For the dense NiAl coating, the formation of a protective Al_2O_3 scale on the coating surface resulted in in-situ healing of inter-splat interfaces during the isothermal oxidation. The healing leads to the transformation of inter-splat oxide scales into a discontinuous distribution of Al_2O_3 particles, which further benefits the supply of sufficient Al for continuous thermal growth of the surface Al_2O_3 scale and strengthens adhesion for long-term effective protection of the metal substrate.

METHODS

Powder preparation

The Ni/Al and Ni/Al/2wt.%diamond composite powders were prepared by the ball milling process. First, the electrolytic Ni powder (99.9 wt%, $-50\ \mu\text{m}$, Xingrongyuan Ltd, Beijing, China) and spherical Al powder (99.9 wt%, $-50\ \mu\text{m}$, Quanxin Materials Ltd, Sichuan, China) with the particle size of approximately $50\ \mu\text{m}$ were mixed in a Ni/Al atomic ratio of 1:1. Without or with 2 wt.% diamond powder (99.9 wt%, Deke Ltd, Beijing, China) was added to the Ni/Al powder mixed in an automatic mixer for 2 h to obtain uniform mixtures. Then, the powders were mixed with stainless balls of 6 mm at a ball-to-powder charge mass ratio of 10:1 and were milled in a planetary ball mill (YXQM-20L) at a rotation speed of 180 rpm for 5 h. To prevent the oxidation of the powders, argon was filled into the cylinder of the mill during the milling operation. To facilitate the generation of ultra-high temperature molten particles, feedstock powder particles with a size range from 30 to $50\ \mu\text{m}$ were used in this study to deposit coatings by APS. Figure 13 shows the cross-sectional microstructures and morphology of the mechanically alloyed Ni/Al and Ni/Al/2 wt.%Diamond composite powders. It

can be observed that the powders have an irregular shape and consist of alternately welded fine Ni and Al layers. Additionally, the diamond was uniformly distributed within the powders (Fig. 13d).

Coating preparation and isothermal oxidation test

The NiAl intermetallic coatings were deposited onto a grit-blasted GH4202 substrate by APS of the Ni/Al composite powders without diamond or with a diamond content of 2 wt.% using a commercial plasma spray system (80 kW, Jiujiang, China) in an ambient atmosphere. The coatings were referred to as the NA0 coating and NA1 coating, respectively. The nominal composition (in wt%) of GH4202 superalloy is listed in Table 2. The spray power and spray distance were set as 46 kW and 80 mm, respectively. The flow rates of the primary gas (Ar) and the secondary gas (H_2) were set as 45 and 6 L/min, respectively. Subsequently, the GH4202 substrate and prepared coatings were cut into $10\ \text{mm} \times 10\ \text{mm}$ sizes for the oxidation test. Isothermal oxidation tests were carried out at 900°C in the air using a muffle furnace for different holding durations of 1 h, 10 h, 50 h, 100 h, 200 h, and 500 h. To eliminate the surface oxide layer formed during APS and obtain the same surface finish for all samples, all the specimens were ground using silicon carbide abrasive papers with a grit size of 1500.

Characterization

The morphology and microstructure of the powders and coatings were characterized by scanning electron microscope (SEM, MIRA 3 LMH, TESCAN). The oxygen content of the coatings was measured by oxygen, nitrogen, and hydrogen analyzer (ELEMENTARC ONH-p). The porosity and oxide inclusion content of the coatings as well as the thickness of the oxide scale layers on the coating surface subjected to isothermal oxidation for different durations were measured by ImageJ software using SEM images of polished cross-sections of coatings. To protect the oxides scale from spalling off during the cutting and polishing of the specimen for metallographic sample preparation, Ni plating was employed to deposit a protection layer of Ni on the coating surface. The elemental composition was analyzed using an attached EDS to SEM. The phase composition of the coatings were examined by an X-ray diffractometer (XRD, D8 ADVANCE) using a Cu/K α X-ray source with a step size of 0.1° .

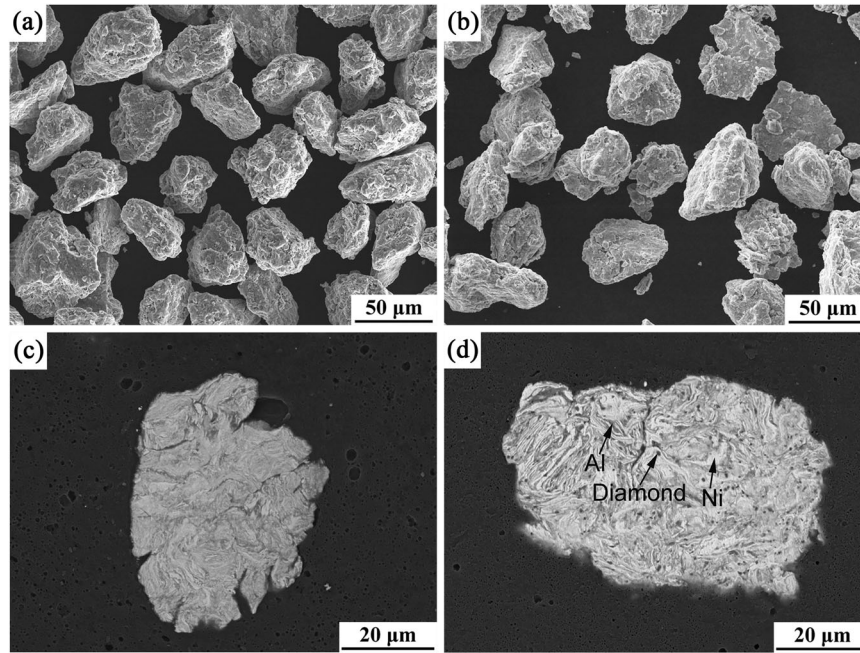


Fig. 13 Cross-sectional microstructures and morphology of the mechanically milled powders. **a, c** Ni/Al composite powder; **b, d** Ni/Al/2wt% Diamond composite powder.

Table 2. Nominal composition of GH4202 superalloy (wt.%).

Ni	Cr	W	Mo	Fe	Ti	Al	Mn	C	B	Si	Ce	S	P
Bal.	17.0– 20.0	4.0– 5.0	4.0– 5.0	≤4.0	2.2– 2.8	1.0– 1.5	≤0.5	≤0.08	≤0.01	≤0.6	≤0.01	≤0.01	≤0.015

DATA AVAILABILITY

All data generated or analyzed during this study are available from the author upon reasonable request.

Received: 8 March 2023; Accepted: 23 July 2023;

Published online: 02 August 2023

REFERENCES

- Chen, Z., Wu, M., Pei, Y., Li, S. & Gong, S. Study on abnormal hot corrosion behavior of nickel-based single-crystal superalloy at 900 °C after drilling. *NPJ Mater. Degrad.* **5**, 21 (2021).
- Li, W. et al. Improvement of cyclic oxidation resistance of a β -(Ni, Pt) Al coating by the addition of Ni/Ni-Re layer at 1150 °C. *Corros. Sci.* **207**, 110486 (2022).
- Sivakumar, R. & Mordike, B. L. High temperature coatings for gas turbine blades: a review. *Surf. Coat. Technol.* **37**, 139–160 (1989).
- Zhang, X. et al. Al₂O₃-modified PS-PVD 7YSZ thermal barrier coatings for advanced gas-turbine engines. *NPJ Mater. Degrad.* **4**, 31 (2020).
- Liu, R. et al. Recognition of NiCrAlY coating based on convolutional neural network. *NPJ Mater. Degrad.* **6**, 7 (2022).
- Shi, J. et al. Isothermal oxidation and TGO growth behavior of NiCoCrAlY-YSZ thermal barrier coatings on a Ni-based superalloy. *J. Alloy. Compd.* **844**, 156093 (2020).
- Zhong, J. et al. Thermal cyclic oxidation and interdiffusion of NiCoCrAlYHf coating on a Ni-based single crystal superalloy. *J. Alloy. Compd.* **657**, 616–625 (2016).
- Yu, Y. et al. Oxidation resistance at 900 °C of porous NiAl-Cr intermetallics synthesized via rapid thermal explosion reaction. *J. Alloy. Compd.* **906**, 164374 (2022).
- Maznoy, A. et al. Predicting oxidation-limited lifetime of Ni-Al-Cr porous radiant burners made by combustion synthesis. *J. Alloy. Compd.* **934**, 167885 (2023).
- Roy, I., Ray, P. K. & Balasubramanian, G. Examining oxidation in beta-NiAl and beta-NiAl plus Hf alloys by stochastic cellular automata simulations. *NPJ Mater. Degrad.* **5**, 55 (2011).
- Kitaoka, S., Kuroyama, T., Matsumoto, M., Kitazawa, R. & Kagawa, Y. Control of polymorphism in Al₂O₃ scale formed by oxidation of alumina-forming alloys. *Corros. Sci.* **52**, 429–434 (2010).
- Li, X. et al. Effect of Al₂O₃ scales from pre-oxidation on the microstructural evolution and phase transition of NiAlHf coatings at 1200 °C. *Surf. Coat. Technol.* **433**, 128119 (2022).
- Hardwicke, C. U. & Lau, Y. C. Advances in thermal spray coatings for gas turbines and energy generation: a review. *J. Thermal Spray Technol.* **22**, 564–576 (2013).
- Zakeri, A., Bahmani, E. & Ramazani, A. A review on the enhancement of mechanical and tribological properties of MCrAlY coatings reinforced by dispersed micro and nanoparticles. *Energies* **15**, 1914 (2022).
- Kiryç, M., Kurumlu, D., Eggeler, G., Vaßen, R. & Marginean, G. On the sliding wear and solid particle erosion behaviour of HVOF-sprayed CoNiCrAlY coatings and NiCrCoTi substrates in dependence of the oxidation dwell time at 900 °C. *Surf. Coat. Technol.* **453**, 129137 (2023).
- Rhys-Jones, T. N. Coatings for blade and vane applications in gas turbines. *Corros. Sci.* **29**, 623–646 (1989).
- Aghayar, Y., Khorasanian, M. & Lotfi, B. High temperature behavior of diffusion aluminide coating on alloy 600 superalloy. *Mater. High Temp.* **35**, 343–354 (2018).
- Li, S. et al. Effect of pre-oxidation on the failure mechanisms of EB-PVD thermal barrier coatings with (Ni, Pt) Al bond coats. *Corros. Sci.* **193**, 109873 (2021).
- Bai, M., Reddy, L. & Hussain, T. Experimental and thermodynamic investigations on the chlorine-induced corrosion of HVOF thermal sprayed NiAl coatings and 304 stainless steels at 700 °C. *Corros. Sci.* **135**, 147–157 (2018).
- Hu, L. et al. A robust, hydrophobic CeO₂/NiCoCrAlY composite coating with excellent thermal stability and corrosion resistance prepared by air plasma spray. *J. Alloy. Compd.* **861**, 158623 (2021).
- Zhao, C. et al. Investigation on the performance of air plasma sprayed thermal barrier coating with Lu/Hf-doped NiAl bond coat. *Surf. Coat. Technol.* **360**, 140–152 (2019).
- Sadeghimeresht, E., Markocsan, N. & Nylén, P. A comparative study on Ni-based coatings prepared by HVOF, HVOF, and APS methods for corrosion protection applications. *J. Thermal Spray Technol.* **25**, 1604–1616 (2016).

23. Di Ferdinando, M. et al. Isothermal oxidation resistance comparison between air plasma sprayed, vacuum plasma sprayed and high velocity oxygen fuel sprayed CoNiCrAlY bond coats. *Surf. Coat. Technol.* **204**, 2499–2503 (2010).
24. Chen, J. Z., Herman, H. & Safai, S. Evaluation of NiAl and NiAl-B deposited by vacuum plasma spray. *J. Thermal Spray Technol.* **2**, 357–361 (1993).
25. Orban, R. L., Lucaci, M., Rosso, M. & Grande, M. A. NiAl oxidation and corrosion resistant coatings obtained by thermal spraying[C]//Advanced materials research. *Trans Tech Publications Ltd.* **23**, 273–276 (2007).
26. Dong, X. Y., Luo, X. T., Ge, Y. & Li, C. J. Enhancing the hot-corrosion resistance of atmospheric plasma sprayed Ni-based coatings by adding a deoxidizer. *Mater. Des.* **211**, 110154 (2021).
27. Zhang, L., Wang, D., Liao, X. J., Luo, X. T., & Li, C. J. The influence of diamond addition to NiAl powder on oxidation behavior of NiAl during plasma spraying for high performance oxide-free NiAl intermetallic coating[C]//ITSC2021. *ASM Int.* 447–453 (2021).
28. Cao, J., Zhang, J., Hua, Y., Chen, R. & Ye, Y. Improving the high temperature oxidation resistance of Ni-based superalloy GH202 induced by laser shock processing. *J. Mater. Process Technol.* **243**, 31–39 (2017).
29. Li, B. et al. Effect of Cr element on the microstructure and oxidation resistance of novel NiAl-based high temperature lubricating composites. *Corros. Sci.* **188**, 109554 (2021).
30. Shirvani, K., Firouzi, S. & Rashidghamat, A. Microstructures and cyclic oxidation behaviour of Pt-free and low-Pt NiAl coatings on the Ni-base superalloy Rene-80. *Corros. Sci.* **55**, 378–384 (2012).
31. Patterson, T., Leon, A., Jayaraj, B., Liu, J. & Sohn, Y. H. Thermal cyclic lifetime and oxidation behavior of air plasma sprayed CoNiCrAlY bond coats for thermal barrier coatings. *Surf. Coat. Technol.* **203**, 437–441 (2008).
32. Zou, Z. et al. Role of internal oxidation on the failure of air plasma sprayed thermal barrier coatings with a double-layered bond coat. *Surf. Coat. Technol.* **319**, 370–377 (2017).
33. Niranatumpom, P., Ponton, C. B. & Evans, H. E. The failure of protective oxides on plasma-sprayed NiCrAlY overlay coatings. *Oxid. Met* **53**, 241–258 (2000).
34. Nijdam, T. J., Jeurgens, L. P. H. & Sloof, W. G. Promoting exclusive α -Al₂O₃ growth upon high-temperature oxidation of NiCrAl alloys: experiment versus model predictions. *Acta Mater* **53**, 1643–1653 (2005).
35. Li, W. et al. The role of Re in effecting isothermal oxidation behavior of β - (Ni, Pt) Al coating on a Ni-based single crystal superalloy. *Corros. Sci.* **176**, 108892 (2020).
36. Susan, D. F. & Marder, A. R. Oxidation of Ni–Al-base electrodeposited composite coatings. I: oxidation kinetics and morphology at 800 °C. *Oxid. Met* **57**, 131–157 (2002).
37. Brennehan, J. et al. Oxidation behavior of GTD111 Ni-based superalloy at 900 °C in air. *Corros. Sci.* **100**, 267–274 (2015).
38. Teng, J. et al. Influence of Ti addition on oxidation behavior of Ni-Cr-W-based superalloys. *Corros. Sci.* **193**, 109882 (2021).
39. Li, D. et al. High temperature oxidation behavior of Ni-based superalloy Nimonic95 and the effect of pre-oxidation treatment. *Vacuum.* **194**, 110582 (2021).
40. Litz, J., Rahmel, A. & Schorr, M. Selective carbide oxidation and internal nitridation of the Ni-base superalloys IN 738 LC and IN 939 in air. *Oxid. Met.* **30**, 95–105 (1988).
41. Li, C. J., Luo, X. T., Dong, X. Y., Zhang, L. & Li, C. X. Recent research advances in plasma spraying of bulk-like dense metal coatings with metallurgically bonded lamellae. *J. Thermal Spray Technol.* **31**, 1–23 (2022).
42. Evans, H. E. & Taylor, M. P. Diffusion cells and chemical failure of MCrAlY bond coats in thermal-barrier coating systems. *Oxid. Met* **55**, 17–34 (2001).
43. Thompson, C. V. Solid-state dewetting of thin films. *Annu. Rev. Mater. Sci.* **42**, 399–434 (2012).
44. Meng, G. H. et al. Highly oxidation resistant and cost effective MCrAlY bond coats prepared by controlled atmosphere heat treatment. *Surf. Coat. Technol.* **347**, 54–65 (2018).
45. Meng, G. H. et al. Vacuum heat treatment mechanisms promoting the adhesion strength of thermally sprayed metallic coatings. *Surf. Coat. Technol.* **344**, 102–110 (2018).
46. Meng, G. H. et al. Highly oxidation resistant MCrAlY bond coats prepared by heat treatment under low oxygen content. *Surf. Coat. Technol.* **368**, 192–201 (2019).

ACKNOWLEDGEMENTS

The present project is financially supported by the Key Program of the National Nature Science Foundation of China (No. U1837201, No. 52031010) and National Science and Technology Major Project (2019-VII-0007–0147).

AUTHOR CONTRIBUTIONS

L.Z: Validation, Formal analysis, Investigation, Writing-Original draft preparation, Data curation. D.W: Methodology, Investigation. R.C: Investigation. X.-J.L: Writing-Review & Editing. X.-T.L: Conceptualization, Writing-Review & Editing. C.-J.L: Conceptualization, Funding acquisition, Supervision, Writing - Review & Editing.

COMPETING INTERESTS

The authors declare no competing interests.

ADDITIONAL INFORMATION

Correspondence and requests for materials should be addressed to Chang-Jiu Li.

Reprints and permission information is available at <http://www.nature.com/reprints>

Publisher's note Springer Nature remains neutral with regard to jurisdictional claims in published maps and institutional affiliations.



Open Access This article is licensed under a Creative Commons Attribution 4.0 International License, which permits use, sharing, adaptation, distribution and reproduction in any medium or format, as long as you give appropriate credit to the original author(s) and the source, provide a link to the Creative Commons license, and indicate if changes were made. The images or other third party material in this article are included in the article's Creative Commons license, unless indicated otherwise in a credit line to the material. If material is not included in the article's Creative Commons license and your intended use is not permitted by statutory regulation or exceeds the permitted use, you will need to obtain permission directly from the copyright holder. To view a copy of this license, visit <http://creativecommons.org/licenses/by/4.0/>.

© The Author(s) 2023